

# Detection of Molecular Clouds in the Interarm of the Flocculent Galaxy NGC 5055

Tomoka TOSAKI,<sup>1</sup> Yasuhiro SHIOYA,<sup>2</sup>

Nario KUNO,<sup>3</sup> Kouichiro NAKANISHI,<sup>3</sup> and Takashi HASEGAWA<sup>1</sup>

<sup>1</sup>*Gunma Astronomical Observatory, Nakayama, Takayama, Agatsuma, Gunma 377-0702*

*tomoka@astron.pref.gunma.jp*

<sup>2</sup>*Tohoku University, Aoba, Sendai, Miyagi 980-8578*

<sup>3</sup>*Nobeyama Radio Observatory, Minamimaki, Minamisaku, Nagano 384-1805*

(Received 2003 January 16; accepted 2003 April 16)

## Abstract

We present high-resolution ( $\sim 4''$ )  $^{12}\text{CO}$  ( $J = 1-0$ ) mapping observations with high-velocity resolution ( $\sim 2.6 \text{ km s}^{-1}$ ) toward the disk of flocculent galaxy NGC 5055, using the Nobeyama Millimeter Array in order to study the physical properties of the molecular clouds in the arm and the interarm. The obtained map shows clumpy structures. Although these are mainly distributed along a spiral arm seen in near-infrared observations, some clouds are located far from the arm, namely in the interarm. These clouds in both the arm and the interarm have a typical size and mass of a few 100 pc and a few  $10^6 M_{\odot}$ , respectively. These correspond to the largest Giant Molecular Cloud (GMC) in our Galaxy, and are slightly smaller than Giant Molecular Associations (GMAs) in the grand design spiral M 51. Their CO flux-based masses show good agreement with their virial masses. A size-velocity dispersion relation is also plotted on an extension of the relation for the Galactic GMCs. These facts suggest that the properties of these clouds are similar to that of the Galactic GMCs. We also found no clear systematic offset between the molecular gas and H II regions unlike M 51. This fact and no existence of GMAs suggest the view that, in NGC 5055, cloud formation and following star formation in both the arm and the interarm are due to enhancement of gas by local fluctuation. On the other hand, in grand design spiral galaxies, such as M 51, GMA formations may occur only in the arm due to a strong density wave also enhanced star formation in GMA formation may also occur. These may control the optical morphology of spiral arms in spiral galaxies.

**Key words:** galaxies: ISM — galaxies: spiral — galaxies: individual (NGC 5055)

## 1. Introduction

Spiral structures are a striking feature of galaxies, and are considered to have a correlation with dense gas formation and/or star formation because spiral structures trace the density wave that is expected to accumulate or compress molecular gas. We can find various morphological types of spiral arms in many galaxies. Elmegreen, Elmegreen (1982) and Elmegreen, Elmegreen (1987) introduced the idea of an arm class as a classification system of spiral arms based on the arm continuity, length, and symmetry, and this may be related to the existence or strength of a density wave. The arm classes have a range from 1 to 12, and are classified into 3 main groups, i.e., flocculent, multiple, and grand design. Flocculent spiral galaxies have short and patchy spiral arms, whereas grand design spiral galaxies show long and continuous spiral arms. Multiple spiral galaxies are located at intermediate type between them.

For the grand design spiral galaxy of M 51, an offset among  $^{12}\text{CO}$ ,  $^{13}\text{CO}$ , and  $\text{H}\alpha$  emissions in spiral arms was found, namely, the  $^{13}\text{CO}$  and  $\text{H}\alpha$  emissions were located at the downstream side of  $^{12}\text{CO}$  (Tosaki et al. 2002; Vogel et al. 1988). These offsets suggest that there is a time delay between an accumulation of gas caused by the density wave and dense gas formation and a following star formation.

On the other hand, recent near-infrared and CO observations showed that there are long, continuous spiral arms in the flocculent galaxy NGC 5055, though they are weaker than those of grand design spiral arms, such as M 51 (Kuno et al. 1997; Thornley, Mundy 1997). They suggest the possibility that density waves of old stars exist in spiral galaxies universally, even if there is a difference in the strength. This possibility indicates the view that a density wave plays a role for dense gas and star formation in spiral galaxies. However, only a few attempts have so far been made to perform high-resolution observations of molecular gas in the galactic disk, particularly, for flocculent galaxies. In order to investigate the role of density waves, we need information about the molecular cloud properties and star formation in spiral galaxies with different arm classes.

To study the molecular cloud properties in and between spiral arms and to consider the effect of spiral arms on the properties of molecular clouds, we present the results of observations with  $^{12}\text{CO}(J = 1-0)$  emission toward the inner disk of NGC 5055. NGC 5055 is a nearby flocculent spiral galaxy, which has been investigated by several observations with various wavelength: e.g., optical, infrared, radio, and so on. This galaxy shows two weak spiral arms in near-infrared and CO observations, and a kinematic indication of the density wave has been found in the galaxy. Previous studies indicated the existence of large molecular clouds in the central region of NGC 5055, such as GMAs seen in nearby grand-design spiral M 51 (Thornley, Mundy 1997). They found the GMAs on the spiral arm, but not between arms, e.g., interarm.

However, molecular clouds in the disk region of galaxies are supposed to have a smaller velocity dispersion if they are similar to Galactic GMCs. Therefore, if observations with a

**Table 1.** Adopted parameters of NGC 5055.

Parameter	Value
Center position (2000.0)*	13 <sup>h</sup> 15 <sup>m</sup> 49.25 <sup>s</sup> 42°01′49.3″
Morphological type <sup>†</sup>	SA(rs)bc
Systemic Velocity <sup>‡</sup>	504 km s <sup>-1</sup>
Distance <sup>‡</sup>	7.7 Mpc
Position angle <sup>§</sup>	103 ± 6°
Inclination <sup>§</sup>	58 ± 2°

\*: Maoz et al. 1996

†: de Vaucouleurs et al. 1991

‡: Wevers et al. 1986

§: Garcia-Gomez, Athanassoula 1991

higher velocity resolution are carried out, it is expected that we can detect interarm clouds. In consideration of this possibility, we performed observations toward the disk region of NGC 5055 with a velocity resolution of 2.6 km s<sup>-1</sup>, which is very high in extragalactic observations. We present the results as following sections.

The parameters of NGC 5055 are summarized in table 1.

## 2. Observations

We carried out aperture synthesis observations of an arm of NGC 5055 in the <sup>12</sup>CO( $J = 1-0$ ) emission line (rest frequency = 115.271204 GHz) using the Nobeyama Millimeter Array (NMA) during 1999 November – 2000 May. The NMA consists of six 10 m antennas, equipped with SIS receivers. We show the observed field superposed on an optical image of NGC 5055 in figure 1. As a back end, we used a 1024 channel FX spectrocorrelator with a total bandwidth of 32 MHz, corresponding to 83.2 km s<sup>-1</sup> at the <sup>12</sup>CO frequency. The bandpass calibration was done with 3C 279, and 1216+487 was observed every 25 minutes as a phase calibrator. The flux scale of 1216+487 was determined by comparisons with planets of known brightness temperature. The uncertainty in the absolute flux scale is estimated to be ~20%.

The data were reduced using the NRO software package UVPROCII (Tsutsumi et al. 1997), and the final maps were made and CLEANed with the NRAO software package AIPS. The size of the synthesized beam is 4″9 × 3″6, corresponding to about 181 pc × 133 pc in linear scale at the distance of NGC 5055. Velocity-channel maps were made with a velocity width of 2.6 km s<sup>-1</sup>. This is a very high-velocity resolution among observations toward external galaxies, and is effective to detect molecular clouds in disk regions, because molecular clouds in a disk are expected to have a smaller velocity width compared with those in the central regions

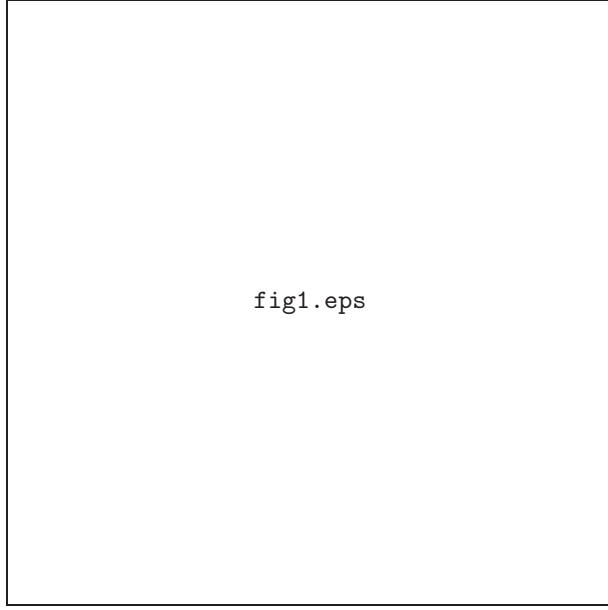


**Fig. 1.** Observed field on the optical image (V-band). The optical image was obtained by Subaru telescope equipped with a Suprime-Cam (Komiyama et al. 2000).

of galaxies.

We measured the flux at a position near to the center of F.O.V,  $(\delta R.A., \delta Decl) = (-30'', -28'')$ , which is the same position as the observed points by 45 m telescope, to estimate the missing flux of our interferometric observations. We deconvolved to the same resolution,  $17''$ , as the 45 m data (Kuno et al. 1997). The measured flux of NMA,  $67 \text{ Jy km s}^{-1}$ , is consistent with the 45 m data,  $65 \text{ Jy km s}^{-1}$ , considering the errors of the flux scale,  $\sim 20\%$ . The line profile was also very similar to that by the 45 m data. This indicates that the most of the single-dish flux has been recovered by our interferometric observations.

### 3. Results

#### 3.1. Global Distribution and Velocity Field of $^{12}\text{CO}$ Emission

Figure 2 shows the total integrated intensity map of  $^{12}\text{CO}$  emission over a velocity range of  $82.3 \text{ km s}^{-1}$ . We found that the emission is distributed mainly along the spiral arm seen in near-infrared observations (Thornley, Mundy 1997). The distribution of CO emission consists of several clumps with a typical size of a few 100 pc. These clumpy structures seem to be similar to that in a grand design spiral galaxy M 51, which shows clear molecular spiral arms composed of GMAs (Rand, Kulkarni 1990; Tosaki et al. 1994a). However, their sizes are smaller than the GMAs seen in M 51 whose size and mass are 1 kpc and  $10^{7-8} M_{\odot}$ , respectively. We also must note that there are clumps outside of the spiral arm, namely, the interarm. These clumps have the same sizes and intensities as those in the arm. This is unlike M 51. Although M 51 has interarm GMAs as well as on-arm GMAs, the emissions of the interarm GMAs are weaker and

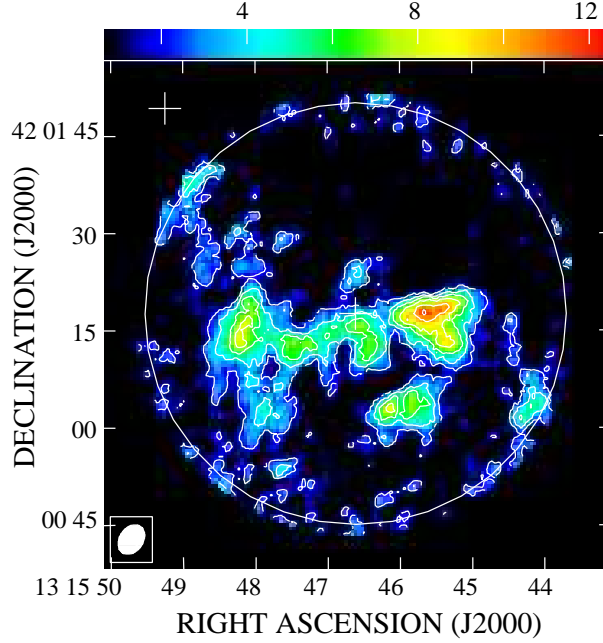


**Fig. 2.** Total integrated intensity map of the  $^{12}\text{CO}$  emission with NMA. The contour interval and lowest contour are  $1 \text{ Jy km s}^{-1} \text{ beam}^{-1}$ , corresponding to noise level. The crosses at the top-left and center indicate the galactic center and center of F.O.V. The F.O.V is indicated as a circle and synthesized beam is plotted at the bottom-left.

also are relatively smaller than the on-arm GMAs (Rand, Kulkarni 1990). Most of clouds in the interarm of M51 are smaller than GMAs and have masses similar to those of GMCs in our Galaxy (Tosaki et al. 1994b).

In figure 3, we present the velocity field of the observed region which traces peaks of CO emission. This figure shows a systematic velocity field derived by galactic rotation in both of the arm and the interarm. If there exists a streaming motion caused by a density wave, we can expect a distortion in the velocity field, such as an S-shape seen in the grand design spiral M 51 with a streaming motion of  $50 - 60 \text{ km s}^{-1}$  (Kuno, Nakai 1997; Aalto et al. 1999). However, we can not see such a distortion in NGC 5055. In other words, we can not find any clear indicator of streaming motion caused by density waves. This indicates that the effect of a density wave on the kinematics in the arm of NGC 5055 is significantly weaker than that in the grand design spiral M 51, even if one exists. This is consistent with the fact that the arm-to-interarm ratio of the NIR arm in NGC 5055, 1.3 (Thornley, Mundy 1997) is smaller than that in M 51, 1.8 – 3, (Rix and Rieke 1993).

We also find the similar systematic velocity shift in the velocity channel maps (figure 4a and b). Each panel of the figure has a velocity range of  $2.6 \text{ km s}^{-1}$ , and emissions are seen in each panel elongated along south-west to north-east, namely, toward the galactic center of NGC 5055. In each velocity channel map, the emissions systematically moved from west to east with increasing of velocity. Our results could not show any clear evidence for streaming

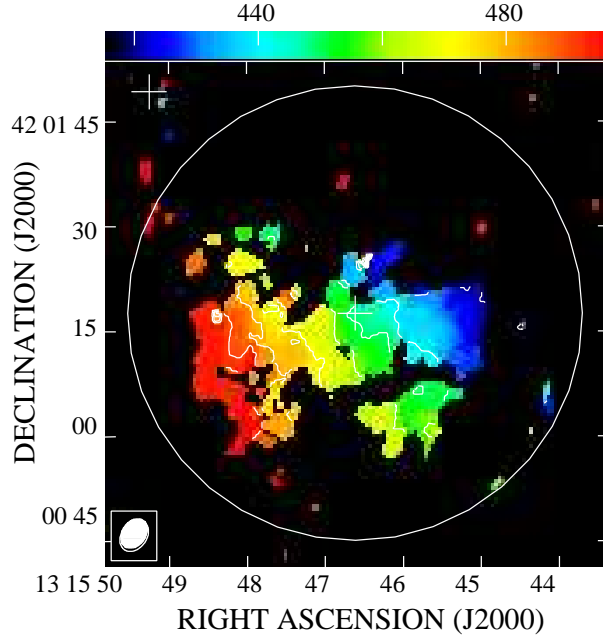


**Fig. 3.** Velocity field. Contour interval is  $10 \text{ km s}^{-1}$ . The crosses and the circle indicate the same as in figure 2.

motion caused by a density wave in NGC 5055.

Figure 5 shows the CO distribution superposed on the  $\text{H}\alpha$  image obtained by the Subaru telescope. Although this is not the subtracted continuum (Komiya et al. 2000), no serious problem arises to trace the star forming regions. In this figure, although some star-forming regions are located near to the spiral arm, we could not find any systematic offset between the CO and  $\text{H}\alpha$  emissions, unlike M 51. A clear offset between the CO and  $\text{H}\alpha$  emissions was found in the grand design spiral M 51 (Vogel et al. 1988), which suggests a time delay between gas accumulation due to the density wave and the massive star formation traced by  $\text{H}\alpha$  emission. In NGC 5055, we could not find such an offset, indicating no systematical time delay between the gas accumulation and star formation. There are clouds associated both with and without massive star-forming regions in both the arm and the interarm of NGC 5055.

### 3.2. *Molecular Clouds in the Arm and the Interarm*

#### 3.2.1. *Identification of clouds*

We identified twelve individual molecular clouds determined by the peaks in the total integrated intensity map. They are indicated as crosses in figure 5 superposed on the total integrated intensity map and  $\text{H}\alpha$  image. Six clouds are distributed on the spiral arm seen in the NIR image (Thornley, Mundy 1997); five clouds (Nos. 3, 7, 8, 11, and 12) and one cloud (No. 2) are located on the sides downstream and upstream of the NIR arm, respectively.

The line profiles of the individual clouds are shown in figure 6. We must note that the velocity coverage was not complete for five clouds (Nos. 1, 2, 3, 10, and 11). Figure 6 also

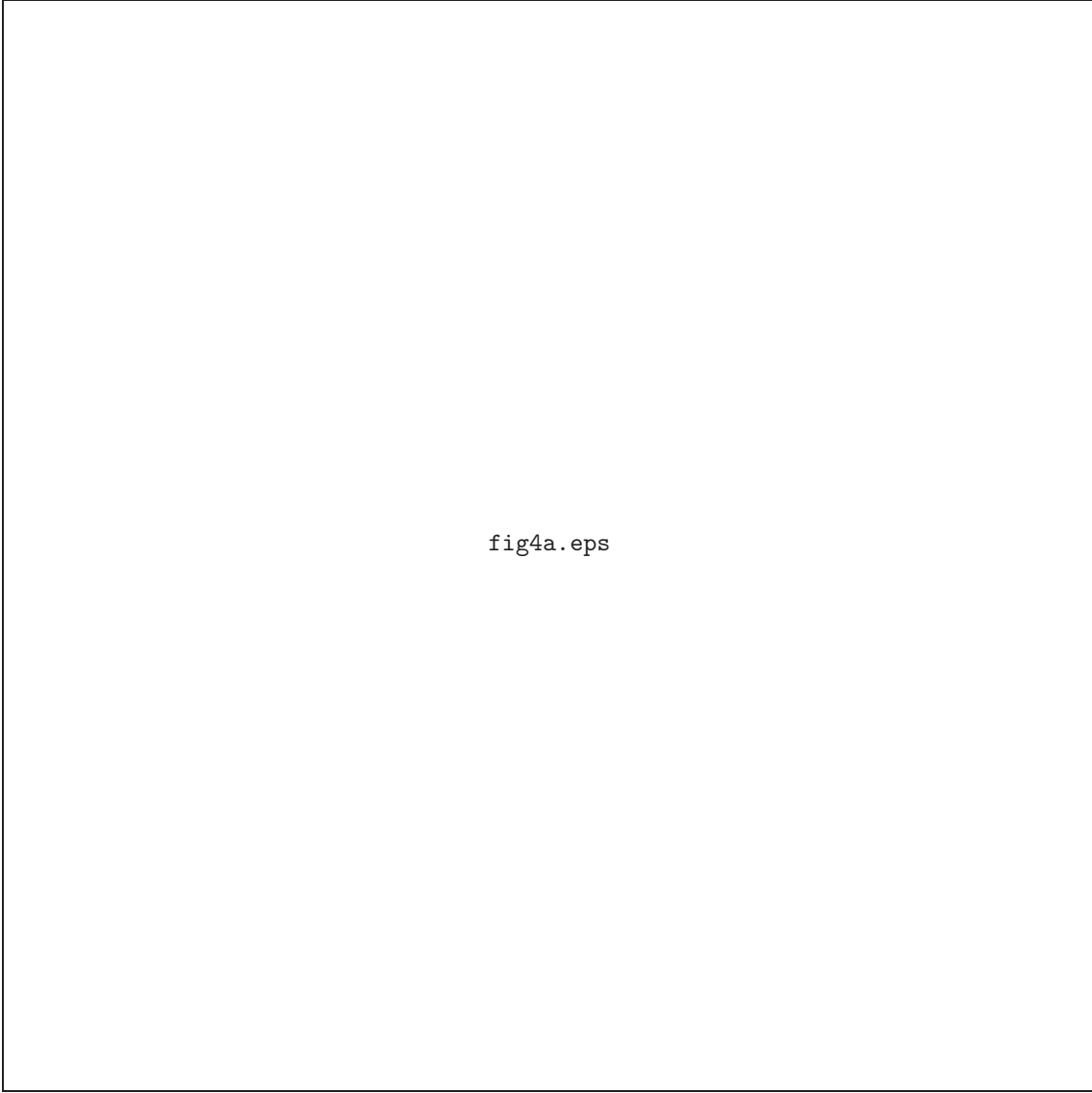


**Fig. 4.** Velocity channel map. The contour interval and lowest contour are  $90 \text{ mJy km s}^{-1}\text{beam}^{-1}$ , corresponding to the noise level. The center velocity of each channel map is indicated at the top-right in each panel. The synthesized beam is at the bottom-left in the top-left panel.

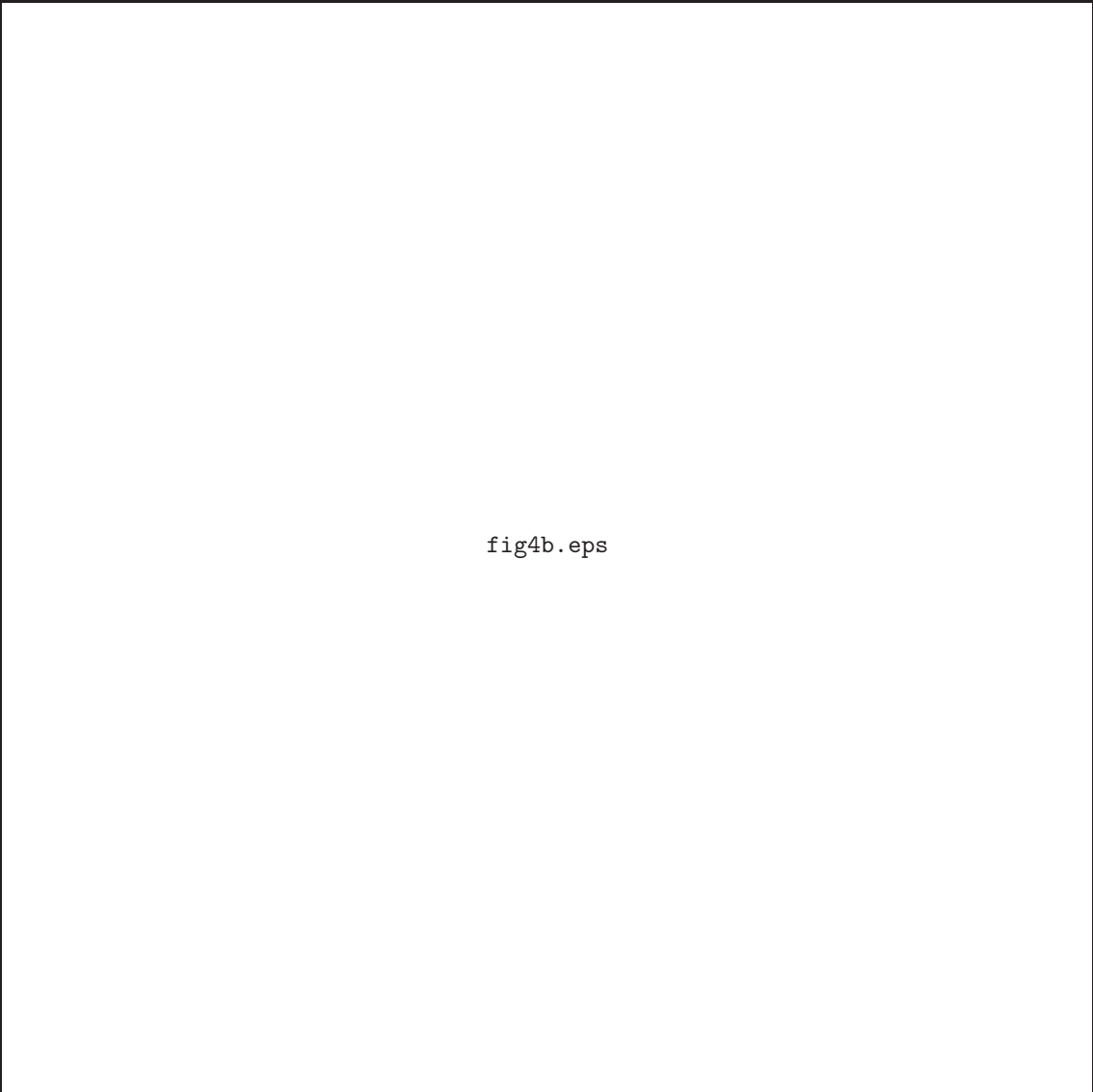


fig4b.eps

indicates that the identified clouds consist of a few velocity components, for example, No. 12 cloud.

### 3.2.2. *Cloud properties*

We summarize the properties of individual molecular clouds in table 2. In the table,  $D$  and  $\Delta v$  are FWHM diameter deconvolved with the beamsize and the FWHM velocity width obtained by a Gaussian fitting, respectively. Since Nos. 2 and 9 clouds have a smaller size than the beamsize, we could not make a deconvolution with the beamsize. We note that the clouds at the edge of F.O.V. can not cover the full velocity range due to the limited velocity coverage. For this reason, the velocity width, CO flux mass, and virial mass of such clouds were obtained as a lower limit (Nos. 1, 2, 3, 10, and 11). However, most of the clouds seem to cover the velocity range containing the peak as shown in figure 6, and are considered not to vary by more



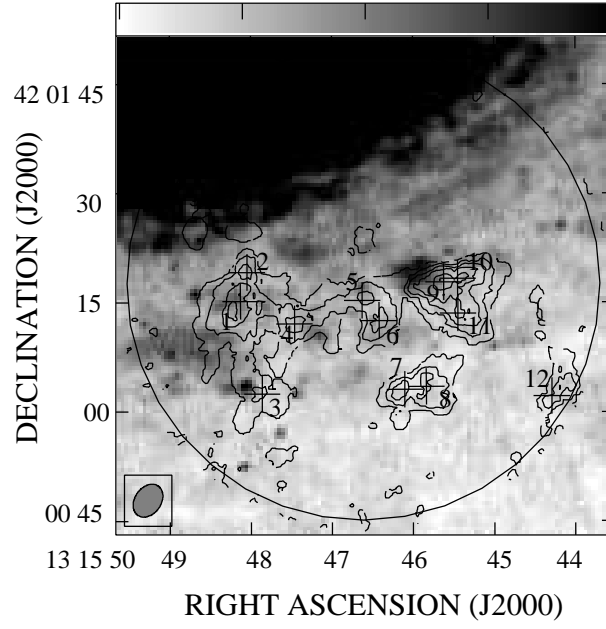


**Fig. 5.** Individual molecular clouds indicated on the total integrated intensity map and H $\alpha$  image.

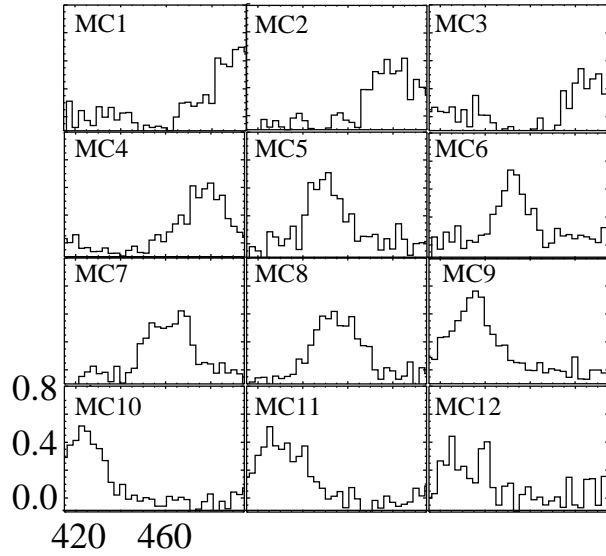


**Fig. 6.** Line profiles of the individual molecular clouds. The horizontal and vertical axes are the velocity ( $\text{km s}^{-1}$ ) and intensity ( $\text{Jy beam}^{-1}$ ), respectively.

than twice.

We calculated both the CO flux-based mass,  $M_{\text{CO}}$ , and the virial mass,  $M_{\text{vir}}$ .  $M_{\text{CO}}$  was derived from the CO flux using the CO-to- $\text{H}_2$  conversion factor in our Galaxy,  $X$ ,  $3 \times 10^{20} \text{cm}^{-2} (\text{K km s}^{-1})^{-1}$  (Strong et al. 1988; Scoville, Sanders 1987). Assuming a  $1/r$  density profile, the virial masses are determined as

$$M_{\text{vir}} = 99[\Delta V(\text{km s}^{-1})]^2 D(\text{pc}). \quad (1)$$

In this table, A/I indicates where the cloud was located. “A”, “IU”, and “ID” mean a cloud in the arm, the upstream side of the arm, and the downstream side of the arm, respectively.

The averaged size of individual clouds is 256 pc, which is larger than the typical size of GMCs in our Galaxy, 40 pc (Scoville, Sanders 1987), but smaller than that of GMAs in M 51 (Rand et al. 1992), 1 kpc. The averaged mass,  $4 \times 10^6 M_{\odot}$  is also larger than that of the typical GMCs, and corresponds to the mass of the largest GMCs in our Galaxy, and is lower than GMAs in M 51,  $\geq 10^7 M_{\odot}$ .

We must point out a possibility that these clouds in NGC 5055 are aggregations of a small cloud, such as GMCs in our Galaxy. In this case, the clouds in NGC 5055 can be resolved to some subparts. However, our information is limited due to the spatial resolution of our observations. If the clouds in NGC 5055 had smaller subparts, then these would be more like GMCs in our Galaxy.

We must also note that these clouds have smaller masses than GMAs seen in a previous study by Thornley, Mundy (1997), which have a typical mass of  $10^7 M_{\odot}$ . This can be caused by a difference in the spatial resolution between our and their observations. The map used to identify GMA had a lower spatial resolution,  $7''$ , than ours. For example, we can see a separation of a few arcsec between the Nos. 9 and 10 clouds in the total map (figure 5). This indicates that each cloud could not be resolved in their map. It seems reasonable that GMA 10 of Thornley, Mundy (1997) corresponds to the sum of the Nos. 9 and 10 identified here. The sum of the masses for two clouds is  $\geq 1.6 \times 10^7 M_{\odot}$ . Although this is slightly smaller than the mass of GMA 10 in Thornley, Mundy (1997),  $3.0$  or  $2.8 \times 10^7 M_{\odot}$ , we can say that both masses agree with each other within the error, considering that this is the lower limit due to the limited velocity coverage. The fact that the clouds identified here have smaller velocity widths than those of GMAs by Thornley, Mundy (1997) supports that their GMAs consist of several components such as the clouds identified here.

We present the  $M_{\text{CO}} - M_{\text{vir}}$  relation of the individual clouds in figure 7. We find that the  $M_{\text{vir}}$  of the individual clouds are comparable to  $M_{\text{CO}}$  in figure 7 within a factor of  $\sim 2$ . If the  $M_{\text{vir}}$  is regarded as being a true mass of clouds, this indicates that we can use the same  $X$  value in NGC 5055 as that of our Galaxy. The  $X$  value depends on the temperature, density, and metallicity of molecular clouds (e.g., Arimoto et al. 1996; Sakamoto 1996; Wilson 1995). The  $X$  decreases with increasing temperature and increases with density, and has a larger value

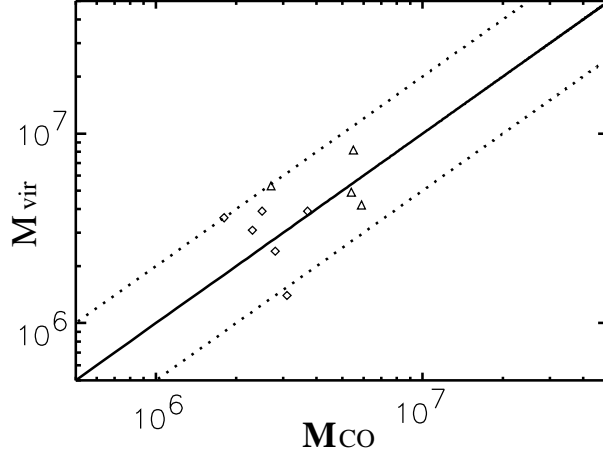


**Fig. 7.**  $M_{\text{CO}}$  vs.  $M_{\text{vir}}$  of the individual molecular clouds. The clouds with a lower limit are indicated as triangles and the rest of the clouds as diamonds. The solid line shows  $M_{\text{CO}} = M_{\text{vir}}$ , and the dotted lines show  $M_{\text{CO}} = 2 \times M_{\text{vir}}$  and  $M_{\text{CO}} = M_{\text{vir}}/2$ .

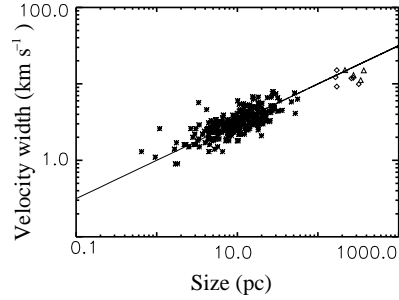
in high metallicity than low metallicity (cf. Wilson, Scoville 1990). For example, the galactic center in our Galaxy shows a smaller  $X$  than that of GMCs in the Galactic plane. This seems to be reflected to high temperature and high density in the Galactic center (Dahmen et al. 1998). Starburst galaxies also have a lower value, indicating that they have different properties from our Galaxy (Aalto et al. 1995), i.e., a higher temperature and density in the clouds. On the other hand, high-latitude clouds showed various  $X$  (Magnani et al. 1998). This may reflect the abundance of CO in the clouds. Considering them, the fact that  $M_{\text{CO}}$  is comparable to  $M_{\text{vir}}$  indicates that these properties of molecular clouds in NGC 5055 are not significantly different from those in our Galaxy.

Figure 8 shows size–velocity relation of individual clouds along with those of GMCs in our Galaxy (Sanders et al. 1985). This figure indicates that although the individual clouds identified here have larger masses and sizes than GMCs in our Galaxy, they are plotted at the same relation as that of GMCs. This also supports that the molecular clouds in NGC 5055 are similar to those of GMCs in our Galaxy. This relation also may support the view that the clouds identified here are similar to those of GMCs in our Galaxy. Hereafter, we call these clouds GMCs.

Table 2 also gives the averaged values of size,  $\Delta v$ ,  $M_{\text{CO}}$ , and  $M_{\text{vir}}$  of the clouds in the arm, and the interarm (downstream to arm), respectively. These values are similar to each other. We found no significant difference between the arm and the interarm.

**Table 2.** Properties of the individual molecular clouds.

No.	$\Delta\alpha$ (arcsec)	$\Delta\delta$ (arcsec)	$D$ (pc)	$\Delta v$ (km s <sup>-1</sup> )	$M_{\text{CO}}$ ( $10^6 M_{\odot}$ )	$M_{\text{vir}}$ ( $10^6 M_{\odot}$ )	A/I	H II
1	-12.5	-34.1	370	$\geq 15.0$	$\geq 5.5$	$\geq 8.2$	A	H II
2	-13.4	-30.2	***	$\geq 12.8$	$\geq 1.8$	***	IU	No
3	-15.5	-46.9	276	$\geq 13.9$	$\geq 2.7$	$\geq 5.3$	ID	H II
4	-19.9	-37.2	259	11.8	1.8	3.6	A	H II
5	-29.2	-34.0	320	9.9	2.3	3.1	A	H II
6	-31.5	-36.8	171	9.2	3.1	1.4	A	?
7	-35.1	-46.2	165	12.2	2.8	2.4	ID	No
8	-38.0	-45.8	274	12.0	3.7	3.9	ID	No
9	-40.4	-31.5	***	12.7	10.5	***	A	H II
10	-42.3	-31.0	338	$\geq 11.2$	$\geq 5.9$	$\geq 4.2$	A	?
11	-42.4	-35.8	216	$\geq 15.1$	$\geq 5.4$	$\geq 4.9$	ID	No
12	-55.2	-47.1	171	15.1	2.5	3.9	ID	No
average			256	12.8	4.2	4.1		
A			292	11.6	4.9	4.1		
ID			220	13.7	3.4	4.1		



**Fig. 8.** Size–velocity width relation of the individual GMCs in NGC 5055 and Galactic GMCs. The solid line indicates the relation of  $\delta v = D^{0.5}$ , which were obtained for the Galactic GMCs (Sanders et al. 1985).

## 4. Discussion

### 4.1. GMC formation in the NGC 5055

As mentioned above, there is no difference in the properties of the GMCs between the arm and the interarm in NGC 5055. We also see no systematic offset between the spiral arms of the molecular gas and H $\alpha$  in NGC 5055.

Here, we consider where the GMCs seen in the interarm were formed, namely in the arms or in the interarm. For this purpose, we compare two timescales, i.e., the lifetime of the clouds and the traveling time of the clouds from the arm to the interarm, as follows.

First, we estimated the traveling timescale of the GMCs, i.e., timescale after leaving arm. For example, the GMC seen in the interarm of NGC 5055, No. 7, has a distance of 3.3 kpc from the arm based on a face-on view. Assuming the rotational velocity as 200 km s<sup>-1</sup>, the timescale was estimated to  $1.6 \times 10^7$  years. This is the lower limit because the spiral arm pattern also moves in the same direction.

Next, we estimated the lifetime of the cloud. Since the time lag of the CO and HII region seen in M 51 is  $10^7$  years and there are no GMCs associated with the HII regions, it is thought that the lifetime of the cloud is shorter than this timescale. The timelag of the CO and HII regions in NGC 6951 was also evaluated to be  $10^6$  years (Kohno et al. 1999). It is therefore considered that the lifetime of the clouds are shorter than the traveling time from the arm, and that the interarm GMC was formed in the interarm.

However, there is another way to estimate the lifetime of the cloud. Elmegreen (2000) suggested that the lifetime of cloud was estimated to be comparable with two times dynamical time of a cloud from observations. The dynamical timescale is  $\tau_{\text{dyn}} = (\frac{4}{3}\pi R_{\text{cl}}^3 / GM_{\text{cl}})^{1/2}$ , where  $R_{\text{cl}}$  and  $M_{\text{cl}}$  are the radius and the mass of the cloud, respectively. Adopting values of No. 7 GMC as  $R_{\text{cl}}$  and  $M_{\text{cl}}$ , we obtained the lifetime as  $2 \times \tau_{\text{dyn}} \sim 2.6 \times 10^7$  years. It seems reasonable that the lifetime of the cloud is similar to the above traveling time. Therefore, it is difficult to see whether the interarm GMCs were formed in the arm or in the interarm. In order to clarify this situation, it is necessary to increase the number of samples and to investigate the relationship between the molecular gas and the star-forming regions.

### 4.2. Flocculent vs. Grand Design

Here, we recall no clear systematic offset with the HII region, which is seen in the arm of M 51. This offset indicates that the star formation started on the arm at the same time by a density wave in M 51. In other words, the absence of an offset suggests that the star formation may not have necessarily started at the same time in NGC 5055. We could also find no GMAs on the arm in NGC 5055, unlike the case of M 51. From these facts, we suggest that the density wave in NGC 5055 plays no direct role in either GMA formation or in the star formation; though a density wave plays a role in the accumulation of molecular gas in arms,

arm-to-interarm ratio of molecular gas is not high compared with that of the grand design spiral M 51.

The gravitational instability of a gas disk plays an important role in star and cloud formation (Kennicutt 1989; Elmegreen 1994; Tosaki, Shioya 1997; Shioya et al. 1998; Kohno et al. 2002). It is reasonable that they easily occur on the arm, because the density in the arm is higher than that in the interarm. From these facts, it is possible to build up a hypothesis as follows. In the flocculent galaxy NGC 5055, since the arm-to-interarm ratio of CO is low,  $\sim 2$ , the difference in the gas density between the arm and the interarm is not significantly large. Therefore, the formations of clouds and stars could occur not only in the arm but in the interarm due to a local fluctuation of the gas density, though it may occur more easily in the arm.

On the other hand, the grand design spiral M 51 shows a clear offset between the molecular gas and the star-forming regions, though we can find the some star-forming regions in the interarm. M 51 also shows a difference of the molecular clouds between the arm and the interarm (see subsection 3.1). These facts suggest that a strong density wave has an effect on the GMA and the star formation in the case of M 51, unlike NGC 5055. Since the gas density becomes high in the arm due to the accumulation of gas by a strong density wave, we consider the following three scenarios. At first, the gas density is higher than the critical density for a large-scale instability, and GMA formation occurs due to the instability in the arms of M51 (Elmegreen 1994). Once GMAs are formed, star formation may follow in the GMAs, as suggested by a comparison of the scale between large-scale instability and star-forming complexes (Elmegreen et al. 1994). Second, GMAs may be formed by the collision of molecular clouds in the arm (Kwan, Valdes 1987). Cloud collisions must also trigger star formation (Larson 1988).. Third, both mechanisms mentioned above work simultaneously.

In a flocculent galaxy, although a weak density wave accumulates gas, the density of the gas becomes not high and not enough for large scale instability or/and collision to occur and trigger star formation. This may produce a different morphology of flocculent and grand design spiral arms. To sum up, in grand design spiral galaxy with a strong density wave, since the star formation is triggered by a strong density wave in the arm, the optical arm with offset from the dust lanes clear, while the star formation in the arm of flocculent galaxy with a weak density wave is not very much. Therefore, we can see no clear optical spiral arm in the flocculent galaxy. We thus propose that the strength of density wave may control the arm morphology.

This is the first example, and we don't yet know whether our findings for NGC 5055 are also applicable to other flocculent galaxies or not. To confirm this scenario, the observation in a large area of NGC 5055 and observations in other galaxies will be needed for a verification. In particular, it will be necessary to observe galaxies with various arm classes and to investigate the relation between the amplitude of the density wave, and the arm morphology.

## 5. Conclusions

We present the results of high-resolution ( $\sim 4''$ )  $^{12}\text{CO}(J = 1-0)$  mapping observations toward the southern bright arm region of the nearby spiral galaxy NGC 5055 carried out with NMA. The velocity resolution of  $2.6 \text{ km s}^{-1}$  was very high in extragalactic observations. The main conclusions are summarized as follows:

1. The molecular clouds are mainly distributed along a spiral arm seen in near-infrared observations. The arm consists of several clumpy structures whose typical size and mass are a few 100 pc and  $10^6 M_{\odot}$ , respectively. The values are comparable to those of GMCs in our Galaxy, and smaller than GMAs in M 51. There is no offset between the molecular spiral arm and the  $\text{H}\alpha$  emission seen in the grand design spiral M 51.

2. We also detected interarm molecular clouds as well as on arm. Their masses and sizes are similar to those on the arm. This differs from grand design spiral M 51, which has GMAs on the arm and no GMAs in the interarm. It is difficult to see whether these interarm clouds were formed in the arm or the interarm based on the argument of the lifetime of clouds.

3. The virial masses of the clouds agree well with the CO flux masses within a factor of 2. We can, therefore, use the CO-to- $\text{H}_2$  conversion factor in our Galaxy, indicating that the properties of clouds, such as the temperature and the density, are not significantly different. The size-velocity width relation was also plotted as the same relation as the Galactic GMCs, supporting this idea.

4. No existence of GMAs and no clear systematic offset between the molecular gas and H II regions suggest the view that, in a flocculent galaxy, cloud formation, and the following star formation occur in both the arm and the interarm due to an enhancement of the gas by a local fluctuation.

### Acknowledgment

We are grateful to the NRO staff for operating and improving of the NMA. We also thank to Drs. Y. Komiyama and H. Fukushima for offering the optical data and giving helpful comments about them. We would like to thank Dr. K. Kohno for useful comment and discussion. Y.S. and K.N. thanks the Japan Society for Promotion of Science (JSPS) Research Fellowships for Young Scientists.

## References

- Aalto, S., Booth, R. S., Black, J. H., & Johansson, L.E.B. 1995, *A&A*, 300, 369
- Aalto, S., Hüttemeister, S., Scoville, N. Z., & Thaddeus, P. 1999, *ApJ*, 522, 165
- Arimoto, N., Sofue, Y., & Tsujimoto, T. 1996, *PASJ*, 48, 275
- Dahmen, G., Hüttemeister, S., Wilson, T.L., & Mauersberger, R. 1998, *A&A*, 331, 959
- de Vaucouleurs, G., de Vaucouleurs, A., Corwin, H. G., Jr., Buta, R. J., Paturel, G., & Fouqué, P.

- 1991, Third Reference Catalogue of Bright Galaxies (New York: Springer-Verlag)
- Elmegreen, B.G. 1994, *ApJ*, 433, 39
- Elmegreen, B.G. 2000, *ApJ*, 530, 277
- Elmegreen, D.M., Elmegreen, B.G. 1982, *MNRAS*, 201, 1021
- Elmegreen, D.M., & Elmegreen, B.G. 1987, *ApJ*, 314, 3
- Elmegreen, D.M., Elmegreen, B.G., Cornelia, L., & Carnella, S. 1994, *ApJ*, 425, 57
- Garcia-Gomez, C., & Athanassoula, E. 1991, *A&AS*, 89, 159
- Kennicutt, R. C., Jr. 1989, *ApJ*, 344, 685
- Kohno, K., Tosaki, T., Matsushita, S., Vila-Vilaró, B., Shibatuka, T., & Kawabe, R. 2002, *PASJ*, 54, 541
- Kohno, K., Kawabe, R., & Vila-Vilaró, B. 1999, *ApJ*, 511, 157
- Komiyama, Y., Yagi, M., Miyazaki, S., Okamura, S., Tamura, S., Fukushima, H., Doi, M., Furusawa, H., et al. 2000, *PASJ*, 52, 93
- Kuno, N., Tosaki, T., Nakai, N., & Nishiyama, K. 1997, *PASJ*, 49, 275
- Kuno, N., & Nakai, N. 1997, *PASJ*, 49, 279
- Kwan, J., & Valdes, F. 1987, *ApJ*, 315, 92
- Larson, R.B., 1988, in *Galactic and Extragalactic Star Formation*, ed. R.E. Pudritz & M. Fich (Dordrecht: Kluwer Academic Publishers), 459
- Magnani, L., Onello, J.S., Adams, N.G., Hartmann, D., & Thaddeus, P. 1998, *ApJ*, 504, 290
- Maoz, D., Filippenko, A. V., Ho, L. C., Macchetto, F. D., Rix, H.-W., Schneider, D. P. 1996, *ApJS*, 107, 215
- Rand, R. J., & Kulkarni, S. R. 1990, *ApJ*, 349, L43
- Rand, R. J., Kulkarni, S. R., & Rice, W. 1992, *ApJ*, 390, 66
- Rix, H.-W., & Rieke, M.J., 1993, *ApJ*, 418, 123
- Sakamoto, S. 1996, *ApJ*, 462, 215
- Sanders, D.B., Scoville, N.Z., & Solomon, P.M. 1985, *ApJ*, 289, 373
- Scoville, N. Z., & Sanders, D. B. 1987, in *Interstellar Processes*, ed. D. J. Hollenbach & H. A. Thronson, Jr. (Dordrecht: Reidel), 21
- Shioya, Y., Tosaki, T., Ohyama, Y., Murayama, T., Yamada, T., Ishizuki, S., & Taniguchi, Y. 1998, *PASJ*, 50, 317
- Strong, A.W., et al. 1988, *A&A*, 207, 1
- Thornley, M.D., & Mundy, L.G. 1997, *ApJ*, 484, 202
- Tosaki, T., Hasegawa, T., Shioya, Y., Kuno, N., & Matsushita, S. 2002, *PASJ*, 54, 209
- Tosaki, T., Kawabe, R., & Taniguchi, Y., 1994a, in *ASP Conf. Ser*, 59, *Astronomy with Millimeter and Submillimeter Wave Interferometry*, IAU Colloq. 140, ed. M. Ishiguro & J. Welch, (San Francisco: ASP), 353
- Tosaki, T., Taniguchi, Y., & Kawabe, R., 1994b, in *ASP Conf. Ser*, 59, *Astronomy with Millimeter and Submillimeter Wave Interferometry*, IAU Colloq. 140, ed. M. Ishiguro & J. Welch, (San Francisco: ASP), 355
- Tosaki, T., & Shioya, Y. 1997, *ApJ*, 484, 664



- Tsutsumi, T., Morita, K.-I., & Umeyama, S., 1997, in ASP Conf. Ser. 125, *Astronomical Data Analysis, Software and System VI.*, ed. G.Hunt & H.E.Payne, (san Fransisco: ASP), 50
- Vogel, S.N., Kulkarni, S.R., & Scoville, N.Z. 1988, *Nature*, 334, 402
- Wevers, B. M. H. R., van der Kruit, P. C., & Allen, R. J. 1986, *A&AS*, 66, 505
- Wilson, C.D. 1995, *ApJ*, 448L, 97
- Wilson, C.D, & Scoville, N. 1990, *ApJ*, 363, 435

This figure "fig1.jpg" is available in "jpg" format from:

<http://arXiv.org/ps/astro-ph/0311427v1>

This figure "fig4a.jpg" is available in "jpg" format from:

<http://arXiv.org/ps/astro-ph/0311427v1>

This figure "fig4b.jpg" is available in "jpg" format from:

<http://arXiv.org/ps/astro-ph/0311427v1>